



OPEN ACCESS

EDITED BY

Yonghui Liu,
Hong Kong Polytechnic University, Hong Kong
SAR, China

REVIEWED BY

Haitao Zhang,
Xi'an Jiaotong University, China
Huaxian Wan,
Southwest Jiaotong University, China

*CORRESPONDENCE

Enze Zhou,
✉ zhou_dky@163.com

RECEIVED 31 October 2023

ACCEPTED 10 January 2024

PUBLISHED 19 January 2024

CITATION

Zhou E, Wang L, Wei R, Liu S and Zhou Y (2024),
A flame combustion model-based wildfire-
induced tripping risk assessment approach of
transmission lines.
Front. Energy Res. 12:1330782.
doi: 10.3389/fenrg.2024.1330782

COPYRIGHT

© 2024 Zhou, Wang, Wei, Liu and Zhou. This is
an open-access article distributed under the
terms of the [Creative Commons Attribution
License \(CC BY\)](#). The use, distribution or
reproduction in other forums is permitted,
provided the original author(s) and the
copyright owner(s) are credited and that the
original publication in this journal is cited, in
accordance with accepted academic practice.
No use, distribution or reproduction is
permitted which does not comply with these
terms.

A flame combustion model-based wildfire-induced tripping risk assessment approach of transmission lines

Enze Zhou^{1*}, Lei Wang¹, Ruizeng Wei¹, Shuqing Liu¹ and You Zhou²

¹Key Laboratory of Power Equipment Reliability Enterprise, Electric Power Research Institute of Guangdong Power Grid Co., Ltd., Guangzhou, Guangdong, China, ²School of Electrical and Information Engineering, Changsha University of Science and Technology, Changsha, Hunan, China

With the intensification of global climate change, the frequency of wildfires has markedly increased, presenting an urgent challenge in assessing tripping failures for power systems. This paper proposes an innovative method to evaluate the spatial wildfire-induced tripping risk of transmission lines based on a flame combustion model. Firstly, Bayes theory is employed to assess the spatial probability of wildfire occurrence. Subsequently, Wang Zhengfei's flame combustion model is utilized to estimate the potential flame height of wildfires along the transmission corridor. Thirdly, the insulation breakdown risk of the transmission line is calculated based on the relative height difference between the flame and the transmission line. Finally, the spatial wildfire-induced tripping risk of the transmission line is then determined by combining the wildfire occurrence probability and the insulation breakdown risk. A case study conducted in Guizhou province, China validates the accuracy of the proposed model. Utilizing ArcGIS, the wildfire occurrence probability distribution in Guizhou is visualized to enhance the efficiency of operation and maintenance. The results indicate that over 80% of wildfire incidents occurred in areas with occurrence probabilities exceeding 50%.

KEYWORDS

wildfire occurrence probability, flame height, insulation breakdown risk, risk level, risk distribution

1 Introduction

Wildfires are on the rise globally due to abnormal climate patterns and traditional fire-usage practices in China. When wildfires encroach upon transmission lines, the risk of tripping increases significantly. This heightened risk is attributed to reduced air insulation between the ground and transmission lines, resulting from elevated temperatures, flame conductivity, and combustion by-products (West, 1979; Naido and Swift, 1993). A notable instance occurred during the 2018 Chinese New Year holiday when the Hunan Power Grid experienced five wildfire-induced tripping failures in just 7 days, causing widespread and severe power outages (T. Zhou et al., 2019). Additionally, on 5 February 2021, a wildfire along the transmission corridor of the 500 kV Laiwu line I in Guangxi province led to multiple tripping instances in quick succession. Consequently, wildfires have become a prominent cause of tripping failures in transmission lines, significantly impacting the safety and stability of power grids (Lu et al., 2016b). Furthermore, wildfires tend to occur during

specific periods due to fire-related customs like moor burns and sacrificial offerings in China. Swift and effective response to these incidents poses a challenge for forestry managers and related utilities. To address this, the Fire Weather Index (FWI) was introduced in 1970 for quantitative assessment of wildfire occurrence risks in wildland areas, encompassing six components that consider fuel moisture and weather conditions (VAN et al., 1987; HOFFMANN et al., 2003; Niu et al., 2006). Subsequently, several wildfire-risk assessment methodologies have been established, such as Australia's Forest Fire Danger Index (FFDI) (William et al., 2003) and Russia's Nesterov Index (NI) (Sherstyukov, 2002). However, the existing indices have predominantly concentrated on assessing the risk of large-scale wildfires in forested areas, overlooking their specific impacts on transmission lines.

In 2016, the State Grid Corporation of China introduced a standard titled "Drawing Guidelines for Region Distribution Map of Wildfires Near Overhead Transmission Lines" (State Grid Corporation of China, 2016). This standard utilized the historical wildfire number index to characterize the influence of human activities on wildfire occurrences. Additionally, vegetation types were categorized, taking into account the impact of burning performance on the insulation of transmission lines (Lu et al., 2016a; Shi et al., 2018; Bian et al., 2021). While offering valuable insights, this standard overlooks the local meteorological and topographic conditions that play a crucial role in influencing vegetation distribution and burning performance. These conditions, consequently, have a significant impact on the real-world spread behavior of wildfires.

To mitigate these constraints, researchers have proposed data mining-based risk assessment models. These models encompass diverse factors: weather conditions, vegetation types, topography, and transmission line structural parameters. Yet, their effectiveness is curbed by sparse, low-quality historical trip failure data under real-world conditions.

(Dian et al., 2016) assessed early warning risks based on the spatial distance between wildfire and transmission line (Liu et al., 2021). introduced a tripping risk method, integrating an adjusted wildfire variation coefficient to gauge transmission line tripping probabilities (Wu et al., 2016). formulated a dynamic wildfire risk model, accounting for wildfire spread direction and speed concerning transmission lines. However, these models overlook the impact of wildfire behaviors on air gap insulation reduction. Wildfire ignition across varied surfaces leads to diverse flame heights and intensities, ultimately compromising transmission line insulation (You et al., 2011). Therefore, it is crucial to consider how distinct fire intensities in different geographic and weather contexts influence the risks associated with line trips.

This study presents an innovative model for assessing wildfire-induced tripping risk of power transmission lines. This model allows for the calculation of potential flame intensity upon the ignition of underlying surfaces. Subsequently, it comprehensively evaluates the impact of two distinct flame scenarios on air gap insulation, thereby facilitating the calculation of insulation breakdown risks. Additionally, the model integrates wildfire occurrence probabilities derived from a Naïve Bayes Network (NBN) to provide a comprehensive assessment of wildfire-induced tripping risks in transmission lines. Guizhou Province in Southwest China is

chosen as the study area. A dataset containing 14 wildfire-related parameters is collected within the study area. This dataset enables the computation of wildfire probabilities and the assessment of wildfire-induced tripping risks. The resulting risk distribution is then mapped using ArcGIS to validate the efficacy and performance of the proposed method.

2 Study area and data

The wildfire-induced tripping risk of transmission line signifies the extent of harm inflicted by wildfire disasters on the operation of transmission lines. This assessment serves as a pivotal guide for devising measures aimed at forestalling wildfires within power grid systems (Castagna et al., 2021). The occurrence of wildfire-induced trips hinges upon two prerequisites. The first one is a wildfire incident occurring near a transmission line. The second is a breakdown occurred between line-to-ground or line-to-line, as the air insulation under the flame condition can no longer withstand the operating voltage of transmission line. Hence, the risk of wildfire-induced trips R_t involves a combination of the wildfire occurrence probability P_f and the insulation breakdown risk R_{t-f} of transmission line, as described by Eq 1.

$$R_t = P_f \times R_{t-f} \quad (1)$$

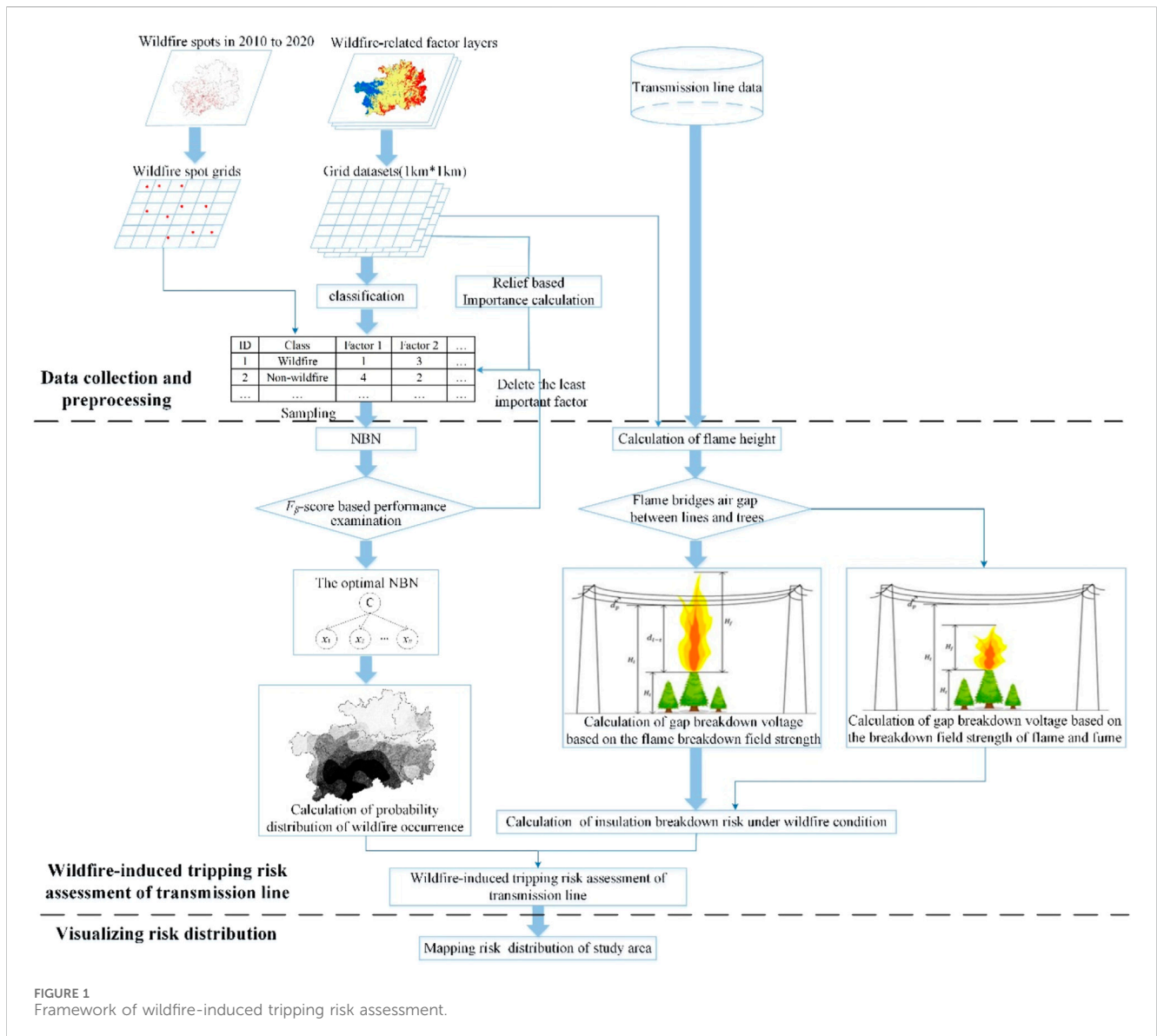
The research framework is shown in Figure 1. In the first phase, the historical fire spot location and wildfire-related factors were collected to form a sample set. And the relief algorithm was used to evaluate the importance of wildfire-related factors. Subsequently, factors with the lowest importance were systematically eliminated. Following this, an optimal Naive Bayesian model was constructed to assess the probability of wildfire occurrence.

In the second phase, meticulous consideration was given to the impact of flame intensity on the gap insulation of transmission line. The insulation breakdown risk was calculated based on distinct scenarios. The assessment of wildfire-induced tripping risk was then conducted by integrating this insulation breakdown risk with the probability of wildfire occurrence.

2.1 Wildfire-related factors

The ignition of wildfires hinge on the presence of fire sources and fuels. Studies have shown that more than 95% of wildfires are ignited by human activities, implying that regions with frequent human activities are more susceptible to both unintentional and deliberate human-induced ignitions (Millington et al., 2008). In this study, five factors including road distance, settlement distance, population density, Gross Domestic Product (GDP) and fire-spot density, are selected to describe the impact of human activities on wildfire occurrence.

The fuel conditions are characterized by the vegetation along the transmission corridors, including land-usage type, vegetation type, normalized difference vegetation index (NDVI) and fuel loads. Besides, both the meteorology and topography have an obvious influence on the vegetation flammability, thereby affecting the ignition and spread of wildfires. The relevant factors include precipitation, temperature, elevation, slope, and aspect (Dios et al., 2021).



2.2 Case study area

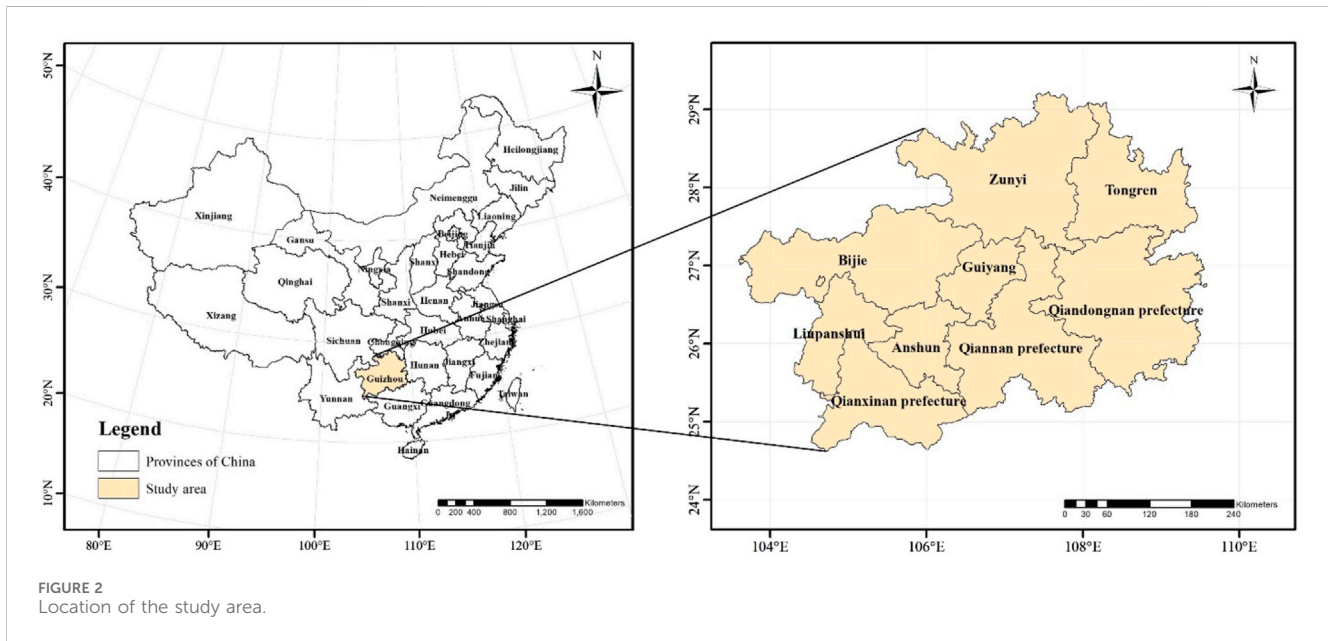
Guizhou Province, located in the Southwest of China (24°37'-29°13'N and 103°36'-109°35'E), as the shown in Figure 2, spans an area of approximately 162,000 km². Characterized by a subtropical monsoon climate, the region provides favorable conditions for the proliferation of dense vegetation, significantly elevating the likelihood of wildfire occurrence. Approximately 200 wildfire incidents were detected annually since 2011 in Guizhou Province, as depicted in Figure 3. Due to the frequent occurrence of wildfires in Guizhou Province and their substantial impact on the power grid, there is an urgent need to develop and implement effective wildfire prevention and control measures.

2.3 Data processing methods

The dataset of fourteen wildfire-related factors was collected for analyzing the occurrence probability distribution of wildfires in the study area. Most of the data were provided by the Resource and

Environmental Science and Data Center of the Chinese Academy of Sciences (<http://www.resdc.cn/Default.aspx>). The information of wildfire incidents from 2010 to 2020 are provided by the China National Meteorological Center. As the general fire-usage habits in a region tend to remain relatively stable over time, the historical fire-spot density was selected to as a feature to reflect the cumulative fire patterns in the region. Specifically, one-third of the dataset from the wildfire incidents (early 2010–2014) was used to compute historical fire-spot density for each grid. And the remaining samples constituted a database for constructing the wildfire risk assessment model. Additionally, the laser point cloud data of transmission corridors is obtained from the China Southern Power Grid Company. The structural parameters of transmission lines, such as the average line-to-ground height, the line-to-line distance, and the line-to-tree height, are calculated based on the laser point cloud data to assess the insulation breakdown risk.

In cases of wildfires occurring within a transmission corridor, the degree of impact on the insulation of transmission lines is directly proportional to the proximity of the wildfire to the transmission line. According to DL/T 1620-2016, the wildfire risk for transmission lines



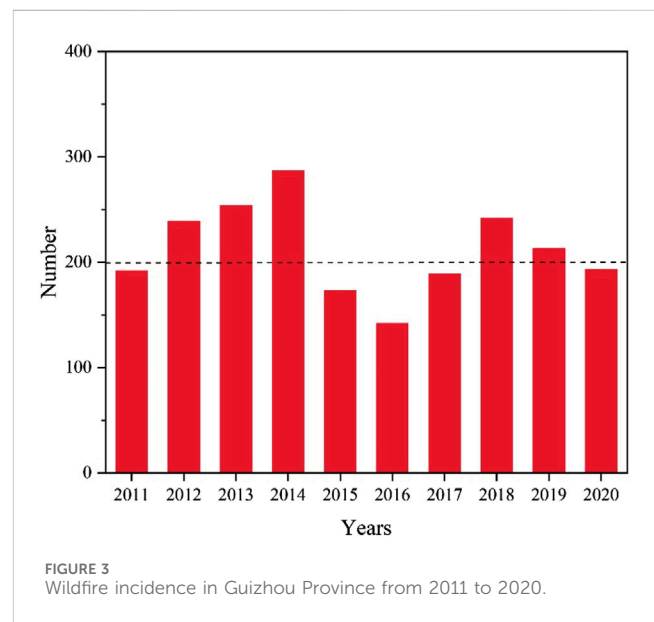
can be evaluated at a range of 1 km (National Energy Administration of China, 2016). Therefore, the study area was subdivided into 1 km × 1 km grids. The data of wildfire-related factors is collected and preprocessed within these grids. For the data with a spatial resolution of larger than 1 km × 1 km, such as annual precipitation and temperature, the kriging method is employed for interpolation. After that, the data of wildfire-related factors are classified into four levels based on the quantile method. The classification standard of wildfire-related factors was listed in Table 1.

3 Methods

3.1 NBN-based wildfire occurrence probability assessment

The Bayes Network (BN) serves as a robust tool for risk assessment, providing an evaluation of hazard likelihood through statistical analysis. Notably, it offers enhanced interpretability compared to other data mining models. Consequently, a BN model was established to evaluate the potential occurrence of wildfires based on wildfire-related factors. This model is described as a graphical cause-and-effect representation, linking variables through conditional probabilities (Requejo et al., 2019).

The BN structure comprises two key components: a directed acyclic graph and conditional probability tables. The directed acyclic graph represents the probabilistic dependencies between pairs of wildfire-related factors or between these factors and wildfire incidence. It is noteworthy that taking into account correlations between factors elevates the computational complexity of the model. However, in certain application scenarios where there is weak correlation between factors or a limited number of factors, assuming independence among factors also allows the model to achieve acceptable performance. To address this, a conditional independence assumption is incorporated, simplifying the BN model into a Naïve



Bayes Network (NBN), as illustrated in Figure 4, where, C is the class node, representing the class of fire or non-fire; Node denotes one of the wildfire-related factors. The conditional probability of C is estimated by Eq. 2.

$$P(C_i | x_1, \dots, x_n) = \frac{P(C_i) \prod_{j=1}^n P(x_j | C_i)}{\sum_{i=1}^2 [P(C_i) \prod_{j=1}^n P(x_j | C_i)]} \quad (2)$$

where C_1 is the class of wildfire; C_2 is the class of non-wildfire.

Firstly, the grids experiencing wildfire incidents between 2015 and 2019 are used as wildfire samples. A corresponding set of grids, equating in number and situated beyond a 3 km radius from the fire-affected areas, is randomly chosen to serve as non-wildfire samples. Subsequently, the sample set is partitioned into a training

TABLE 1 Classification standards of wildfire-related factors.

	Wildfire-related factors	Classes			
		1	2	3	4
Anthropogenic influence	Distance-to-road (m)	<905	905–196	1962–3,403	>3,403
	Distance-to-settlement (m)	<285	285–476	476–772	>772
	Population density (people/km ²)	>220	164–220	105–164	<105
	GDP (10,000yuan/km ²)	>653	375–653	226–375	<226
	Fire-spot density (unit/100 km ² year)	>653	298–653	89–298	<89
Fuel conditions	Land-usage type	High-coverage woodland and grassland	Medium-coverage woodland and grassland	Low-coverage woodland and grassland	Settlements and others
	Vegetation type	Coniferous and mixed forest	Broadleaf forest and shrub	Bushes	Cultivated plants and others
	NDVI	>0.876	0.836–0.876	0.788–0.836	<0.788
	Fuel load (t/km ²)	>23.3	1.3–23.3	1–1.3	<1
Climate	Annual precipitation (mm)	<1,150	1,150–1,422	1,422–1,560	>1,560
	Annual temperature (°C)	>17	16–17	15–16	<15
Topography	Elevation (m)	<813	813–1,047	1,047–1,344	>1,344
	Slope (°)	>20	13–20	8–13	<8
	Aspect	South	East	West	North

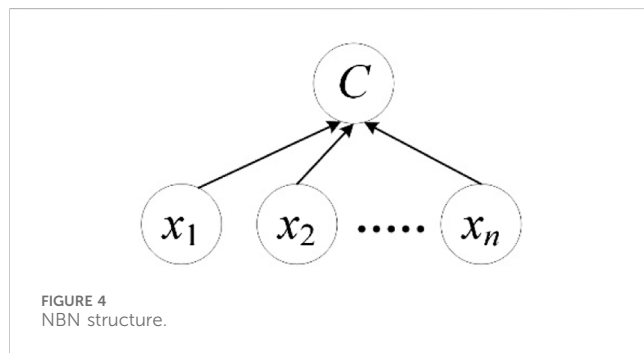


FIGURE 4 NBN structure.

set and a validation set, adhering to a ratio of 7:3. And the wildfire incidents occurring in 2020 are expressly retained to validate the predictive efficacy of the NBN model.

Secondly, the conditional probability tables of wildfire-related factors are calculated by the training set. To mitigate the redundant information, the Relief algorithm is used to rank the importance of wildfire-related factors. The NBN model is optimized by the heuristic search strategy, in which the least important factor is deleted one by one (Chen et al., 2021). During the optimization, a β -score is used to assess the performance of NBN model.

$$F_{\beta} = \frac{(1 + \beta^2)P_r R_e}{\beta^2 P_r + R_e} \quad (3)$$

where P_r and P_e represents the Recall and Precision obtained from the confusion matrix (Woznicki et al., 2019). The β is the relative importance of Recall to Precision. Considering the cost of

wildfire-induced trips, the operational department exhibits a heightened interest in identifying potential hazards effectively. Consequently, there is a greater emphasis on Recall in this study. Thus, we set $\beta = 3$.

The importance rank of wildfire-related factors is shown in Figure 5. The Distance-to-settlement, Vegetation type, Distance-to-road are the top three important factors affecting wildfire occurrence. The Vegetation type determines the flammability of combustibles, affecting the difficulty of wildfire ignition directly. The factors NDVI and fuel load serve as indicators of combustible quantities, predominantly influencing the spread of wildfires while exerting minimal influence on the likelihood of wildfire occurrence.

Considering the fact that more than 95% of wildfires are man-made, the factors representing human activities, such as distance to settlement and distance to road, are particularly important. The importance analysis of wildfire-related factors indicates that the area with abundant flammable plants and human activities is prone to ignition.

As the number of wildfire-related factors decreases from 14 to 8, there is a gradual increase in the F_{β} -score of NBN model, as shown in Figure 6. This observed increment can be attributed to the reduction in interference from redundant factors, enhancing the model's overall performance. However, a noteworthy trend emerges when the factor count diminishes further, specifically from 8 to 5, resulting in a sharp decline in the F_{β} -score. This decline is attributable to the omission of key factors, underscoring their pivotal role in the predictive accuracy of the model. The F_{β} -score attains its pinnacle value of 0.82 when

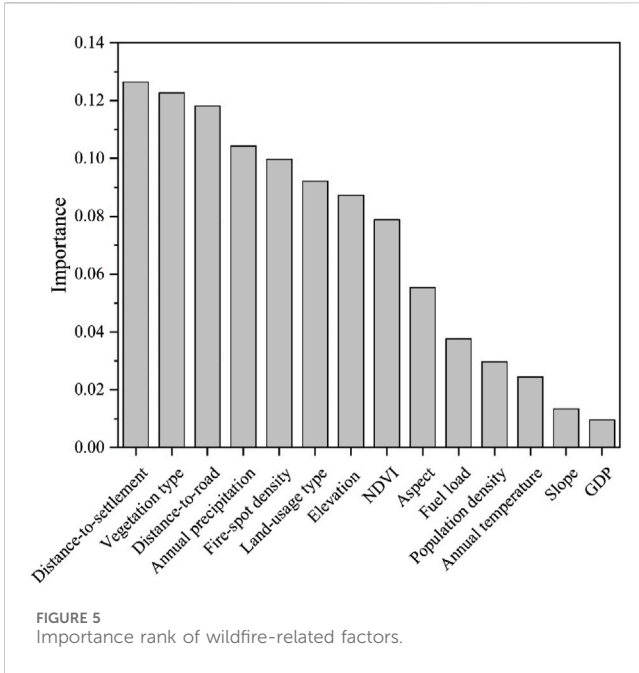


FIGURE 5 Importance rank of wildfire-related factors.

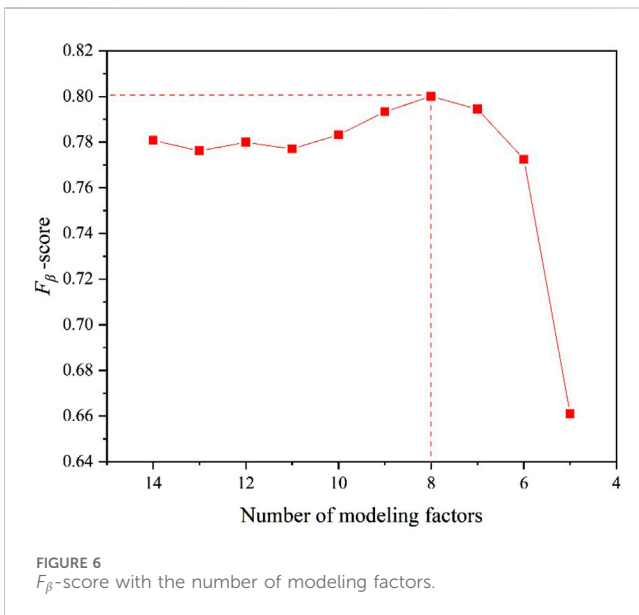


FIGURE 6 F_{β} -score with the number of modeling factors.

employing eight factors. The excluded factors comprise GDP, Slope, Annual temperature, Population density, Fuel load, and Aspect. This omission stems from the observation that GDP and Population density, predominantly reflective of anthropogenic fire-usage habits, exhibit weaker associations with wildfire risk compared to fire spot density. Slope, Fuel load, and Aspect significantly influence wildfire spread, but in this phase emphasizing wildfire occurrence risk assessment, their impact is relatively minor. Despite the close relationship between wildfires and environmental temperature, the limited variance in Annual temperature across diverse regions within a province complicates discerning its influence on wildfire risk. Consequently, the optimized eight wildfire-related factors are

employed to construct the NBN model. The final conditional probability tables are listed in Figure 7.

3.2 Insulation breakdown risk assessment

When a wildfire occurs in a transmission corridor, the reduction of air insulation can induce two kinds of tripping failures of transmission lines, namely, line-to-ground and line-to-line breakdowns. Thus, the insulation breakdown risk R_{t-f} is defined as the greater of the line-to-ground breakdown risk R_g and the line-to-line breakdown risk R_p , as shown in Eqs 4–6.

$$R_{t-f} = \max(R_g, R_p) \tag{4}$$

$$R_g = \frac{\sqrt{2/3} \times U}{U_g} \tag{5}$$

$$R_p = \frac{\sqrt{2} \times U}{U_p} \tag{6}$$

where U is the operating voltage of transmission line; U_g and U_p represent the withstand voltage of the air gap of line-to-ground and of line-to-line under wildfire condition, respectively.

The impact of a flame on the reduction of air gap insulation is strongly related to the combustion strength (You et al., 2011). The combustion process engenders substantial charge carriers through thermal ionization and chemical dissociation, resulting in a high conductivity within the bulk of the flame. Once the flame bridges the entirety of the air gap in either line-to-ground or line-to-line, it is easy to further cause a breakdown, thereby instigating the tripping failure of the transmission line. Even in the cases where the air gap is not fully bridged by the flame, the insulation of the remaining gap would also be greatly reduced by the ash and high temperature in fume (Li et al., 2016). Therefore, the following two different scenarios are considered based on the combustion height of flame.

3.2.1 Flame bridges entirety of air gap

When the height of the flame surpasses that of the transmission line (Figure 8), the entirety of the insulation of both line-to-ground and line-to-line becomes bridged by the flame. Ignoring the insulation of alive trees, whose surface conductivity is generally higher than 0.1 S/m (H. Zhou et al., 2018), the insulations of transmission line are determined by the length of gap and the breakdown field strength of flame E_f .

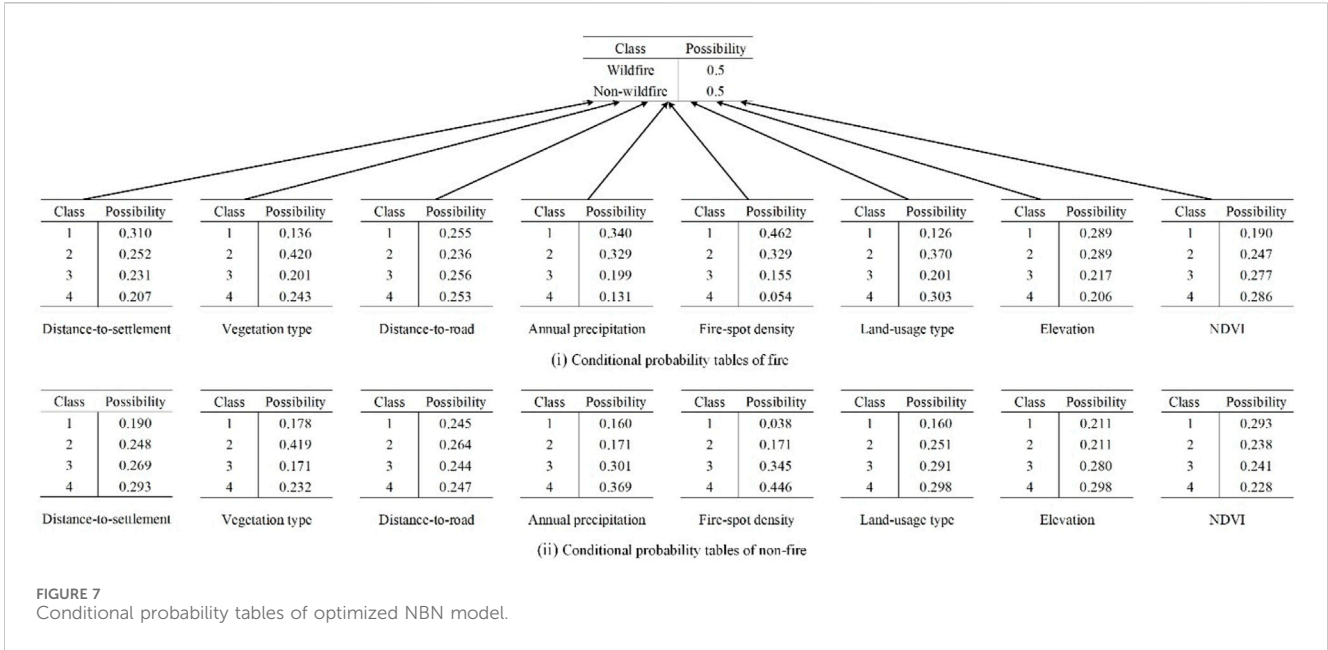
$$U_g = (H_l - H_t) \times E_f = d_{l-t} \times E_f \tag{7}$$

$$U_p = d_p \times E_f \tag{8}$$

where H_l is the minimum height of the transmission line; H_t is the maximum height of trees below the line; d_{l-t} is the minimum length of air gap between transmission line and trees; d_p is the minimum length of air gap between wires of the transmission line. According to the experimental breakdown results of long air gap under flame, E_f is taken as 35 kV/m (Fonseca et al., 1990).

3.2.2 Flame bridges part of air gap

When the height of flame is lower than that of the transmission line, the insulation gap for line-to-ground encompasses a segment



occupied by flames and another by fumes, as shown in Figure 9. The withstand voltage of line-to-ground gap is then determined by

$$U_g = H_f \times E_f + (H_l - H_t - H_f) \times E_s \tag{9}$$

where H_f is the possible height of flame, which can be evaluated by the flame combustion model. And E_s is the average breakdown field strength of fume, which can be obtained by the breakdown field strength amendment of long air gap.

In the most severe case, the air gaps between wires of transmission line are filled wrapped by the fume. Hence, the withstand voltage of line-to-line gap is approximated by

$$U_p = d_p \times E_s \tag{10}$$

3.2.3 Possible flame height H_f

The process of wildfire spread is extremely complicated, depending on the condition of surface fuels and meteorological factors (Benali et al., 2016). Several flame combustion models have been established empirically or semi-empirically, such as McArthur’s model for grassland fires and forest fires in Australia (Noble et al., 1980) and Rothermel’s model for homogeneous and deceased vegetation (Pyne, 1984). Nonetheless, these models are either inadequate for the typical vegetation in Southern of China, or fall short in meeting accuracy criteria due to the requisite homogeneity in practical forest settings. Wang Zhengfei’s model, introduced in 1989, was semi-empirically derived through physical mechanics analysis and based on over 100 field experiments in China (Perry, 1998). Featuring adaptable input parameters, Wang Zhengfei’s model adeptly forecasts wildfire behaviors and finds extensive application in assessing wildfire risks in China.

As mentioned above, the height of flame H_f is an essential parameter that affects the breakdown risk of the air gap. In Wang Zhengfei’s model, the flame height can be estimated by

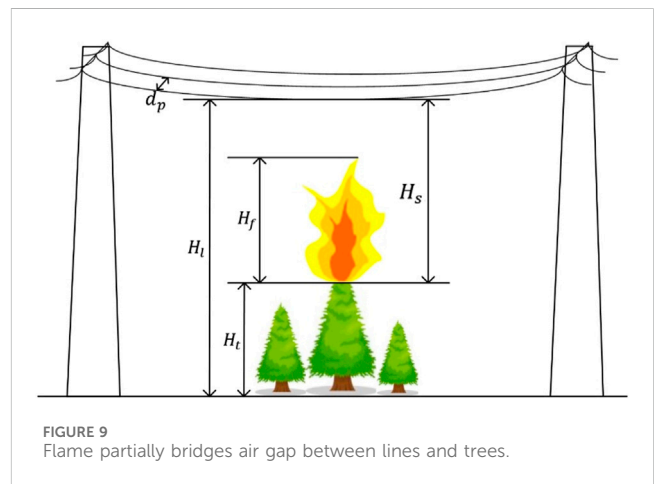
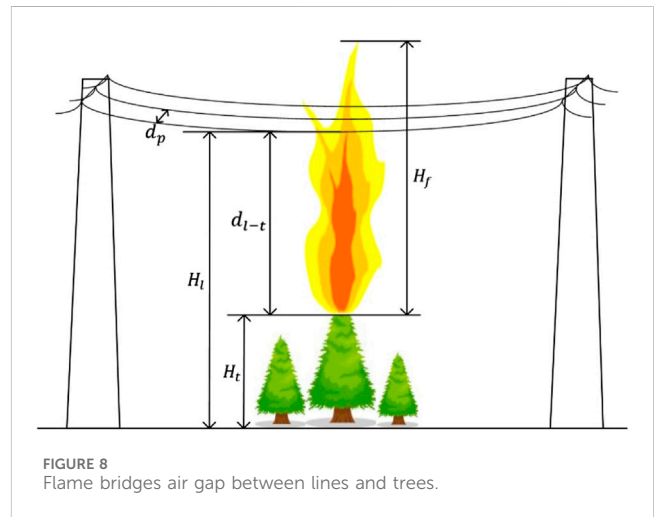


TABLE 2 Values of fuel coefficient (Sun et al., 2012).

Categories	K_c
Water, Settlements, Bare ground, Road	0.0
Arable land	0.1
Mixed forest	0.5
Coniferous forest	1
Grass land	2

$$H_f = \sqrt{I/250} \tag{11}$$

where I is the front-line intensity, which is the energy liberated in time and linear space ($W \cdot m^{-1} \cdot s^{-1}$) during the combustion. The value of front-line intensity is determined by the calorific power q ($kJ \cdot kg^{-1}$) of the combustible material at the underlying surface, the fuel load W ($kg \cdot m^{-2}$) of the combustible material, and the propagating speed of the fire ($m \cdot s^{-1}$) (Byram, 1959; Perry, 1998).

$$I = qWR \tag{12}$$

$$R = K_c K_\phi K_v R_0 \tag{13}$$

where K_c is the fuel coefficient, which depends on the spatial distribution of fuel type, as listed in Table 2; K_ϕ is slope coefficient, and K_v is the wind speed coefficient;

$$K_\phi = e^{3.533 \tan \phi^{1.2}} \tag{14}$$

$$K_v = e^{0.178v} \tag{15}$$

where ϕ is the terrain slope angle; v is the wind speed;

R_0 is a semi-empirical initial spread of wildfire in Wang zhengfei's model. It is defined as the rate of fire spread through a homogeneous fuel field in the absence of wind and topography, and is formulated as (16). In this work, empirical coefficients $\alpha = 0.03$, $\beta = 0.05$, $\gamma = 0.01$, and $\delta = 0.7$.

$$R_0 = \alpha T + \beta F - \gamma H + \delta \tag{16}$$

In summary, the possible height of flame can be estimated by

$$H_f = \sqrt{\frac{qwK_c e^{0.178v+3.533 \tan \phi^{1.2}} (0.03T + 0.05F - 0.01H + 0.7)}{250}} \tag{17}$$

3.2.4 Average breakdown field strength of fume E_s

Even if the flame fails to bridge the gap, the fumes released from the combustion are highly likely to envelop the space around the wires of transmission lines. On one hand, the elevated temperature of the flame decreases the density and humidity of the air within the fume, facilitating the development of electron avalanches (Mphale et al., 2010; Sun et al., 2012). On the other hand, floating particles and ash from the fume drift into the high-electric-field area near the wires, further distorting the electric field distribution and instigating discharge. Hence, based on the adjustments in density and humidity, a particle coefficient K_p is introduced to modify the breakdown strength of air gap (Wang et al., 2011; Li et al., 2016).

$$E_s = K_p K_\sigma K_h E_a \tag{18}$$

where E_s is the average breakdown strength of fume; K_σ and K_h represent the coefficient of density and humidity, respectively; E_a is the breakdown strength of air gap under standard atmospheric conditions (Temperature: 20°C, Humidity: 11 g/m³, Atmospheric pressure: 101.3 kPa).

The triggering effect of ash particles on discharge depends on the type of burning vegetation. Experimental results show that the AC breakdown voltage of the air gap, influenced by the ashes and particles released by the combustion of thatch and fir branch, can reduce to approximately 40% of that observed under the standard atmosphere (Li et al., 2016). Therefore, the particle coefficient K_p is taken as 0.4.

The density coefficient K_σ depends on the relative air density in the fume and can be expressed as

$$K_\sigma = \sigma^m \tag{19}$$

$$\sigma = \frac{(273 + T_a) P_f}{(273 + T_a + \Delta T) P_a} \tag{20}$$

where m is the correction index, which is associated with electrode shape, gap length, voltage type, and other factor, and is simplified to 1; P_a is the ambient pressure, and T_a is the ambient temperature; P_f represent the changed atmospheric pressure above the flame. Assuming that the heating is a long-term process affecting the air above the flame, the local pressure remains essentially unchanged in open space, that is $P_f \approx P_a$; ΔT is the temperature rise of air in the fumes, estimated by the flame combustion model (Heskestad, 1998).

$$\Delta T = \frac{3.9I^{2/3}}{H_s} \tag{21}$$

where H_s is the height of the calculated position relative to the canopy. In the case of line-to-ground breakdown, the median height of the flame is considered, that is $H_s = H_f + 0.5(d_{l-t} + H_f)$. For the line-to-line breakdown, the height is taken as $H_s = d_{l-t}$.

The humidity coefficient of air is expressed as

$$K_h = k^w \tag{22}$$

where w is an exponent parameter, which is related to gap length, electrode shape, voltage type and other factor, and is simplified to 1; k depends on the voltage type and is determined by the ratio of absolute humidity h to the air density δ in the fume. For AC breakdown of air gap, k is obtained by the following equation:

$$k = 1 + 0.012 \left(\frac{h}{\sigma} - 11 \right) \tag{23}$$

To determine the standard breakdown field strength E_a , two different breakdown mechanisms are concerned. For short distance, the breakdown of the air gap is governed by the propagation of streamer. The breakdown field strength E_a is regarded as nearly independent of the gap length, and is assigned a value of 241.39 kV/m. As the gap distance increases, the electric field around the transmission line creates conditions for the inception and propagation of a continuous leader, which exhibits significantly higher conductivity compared to the streamer (Gallimberti, 1979). For air gaps exceeding 4 m, the Rizk semi-empirical model (Rizk, 1989a; Rizk, 1989b) is employed to determine the breakdown strength, as expressed in Eq 24.

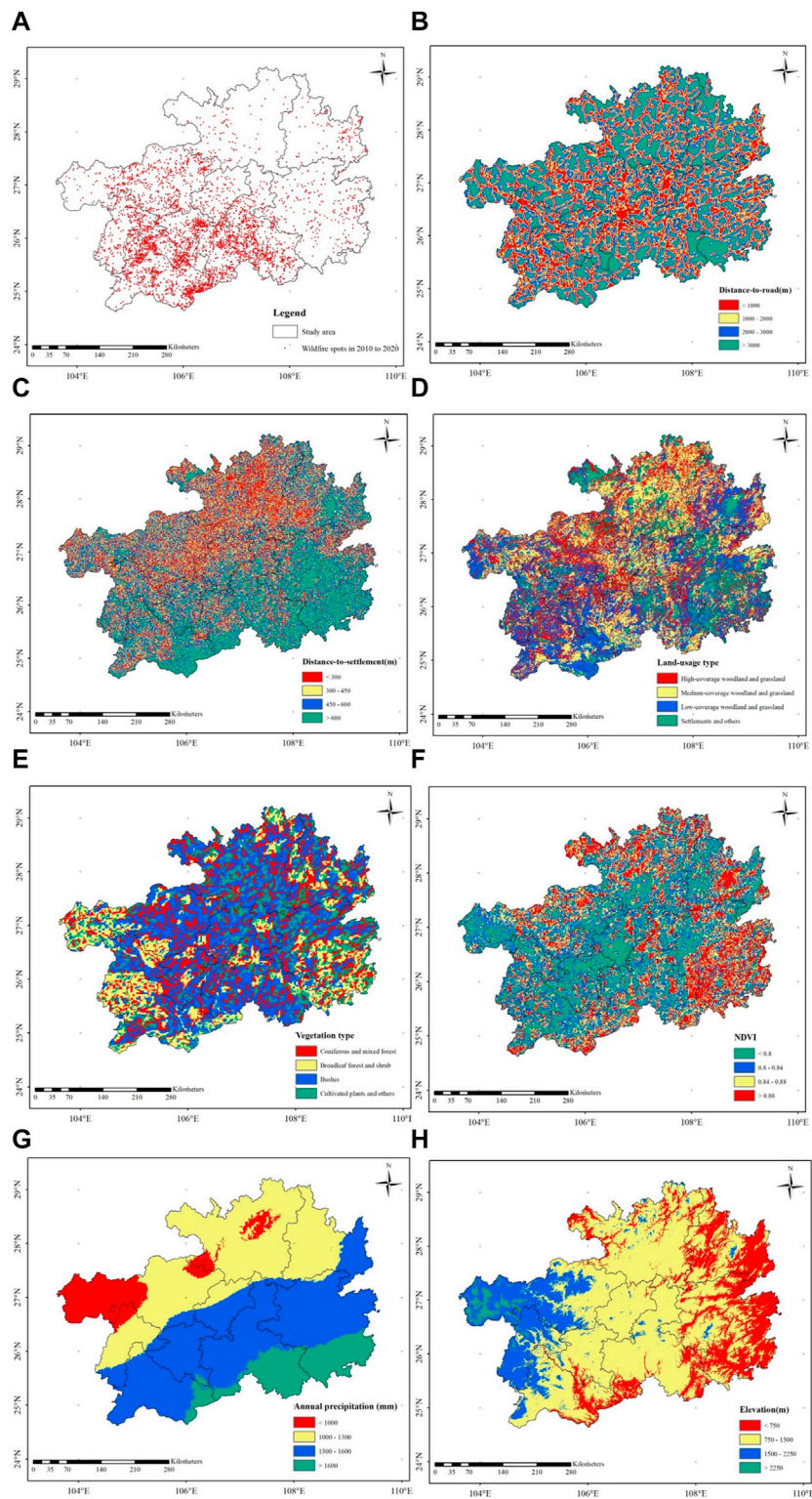


FIGURE 10 Spatial distributions of factors in the study area. (A) Wildfire spots in 2010 to 2020; (B) Distance-to-road; (C) Distance-to-settlement; (D) Land-use type; (E) Vegetation; (F) NDVI; (G) Annual precipitation; (H) Elevation.

$$E_a = \left(\frac{1850 + 59d_s}{1 + 3.89/d_s} + 92 \right) / d_s = \frac{59d_s^2 + 1942d_s + 357.88}{d_s^2 + 3.89d_s} \quad (24)$$

where d_s is the gap length. In summary, the average breakdown strength of fume E_s is expressed as

$$E_s = \begin{cases} \left(0.3472 \left(1 + \frac{3.9I^{2/3}}{273 + T_a} \right)^{-1} + 0.0048h \right) \times \frac{59d_s^2 + 1942d_s + 357.88}{d_s^2 + 3.89d_s}, & d_s \geq 4 \\ \left(0.3472 \left(1 + \frac{3.9I^{2/3}}{273 + T_a} \right)^{-1} + 0.0048h \right) \times 241.39, & d_s < 4 \end{cases} \quad (25)$$

3.3 Spatial distribution of factors in the study area

The spatial distributions of factors are shown in Figure 10. The elevation in Guizhou Province gradually increases from east to west, accompanied by a corresponding rise in precipitation from west to east due to elevation and topography. Predominantly, the area features moderate grassland and woodland, with settlements concentrated in the eastern and northern regions. Consequently, vegetation in the east and north is characterized by cultivated plants and bushes, while the west and south boast significant woodland. The southwest region of Guizhou Province experiences a heightened frequency of wildfires, contrasting with fewer occurrences in the eastern and northern areas. The province’s population centers predominantly lie in the north, contrary to historical fire density. This may be attributed to densely populated cities in the north, making it challenging for fires to escalate into large-scale incidents, as they are promptly detected and artificially extinguished. This underscores the need for increased focus on wildfire prevention and control in the southwest. The intricate nature of the distribution of factors related to wildfires makes it challenging to evaluate the risk of wildfires in specific regions through simplistic regional statistical methods.

4 Results

4.1 Wildfire occurrence probability distribution of study area

The established NBN model was used to calculate the wildfire occurrence probabilities across all grids within the study area. And the results were spatially visualized using ArcGIS 10.5 software with ArcMap module function. During the process of drawing the map, the wildfire occurrence probability is divided into four intervals of (0, 0.25], (0.25,0.5], (0.5,0.75] and (0.75, 1]. And the grids are given different shades of gray from light to dark depending on the intervals, as shown in Figure 11. Regions exhibiting higher probability of wildfire occurrence are primarily concentrated in the southwest zone of Guizhou province. These areas feature a pronounced abundance of fuel loads, thereby providing favorable conditions for ignition. Conversely, the central and northern parts of Guizhou consist predominantly of urban areas characterized by high population density and relatively low vegetation coverage. Consequently, the likelihood of

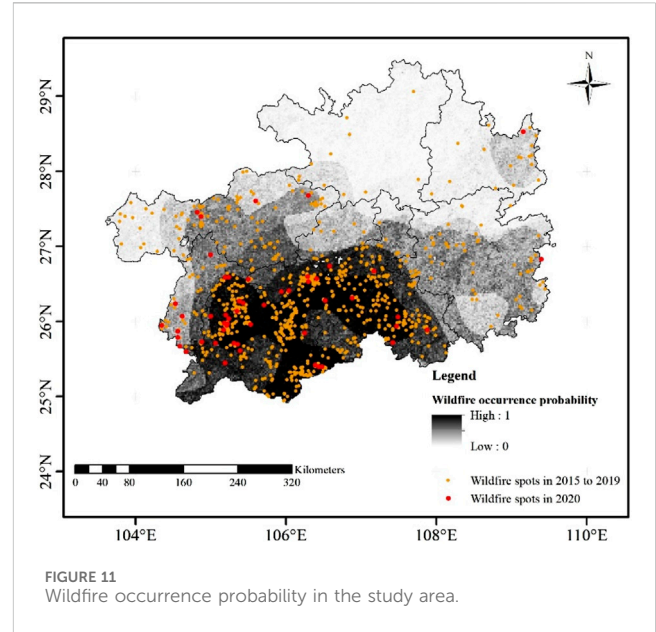
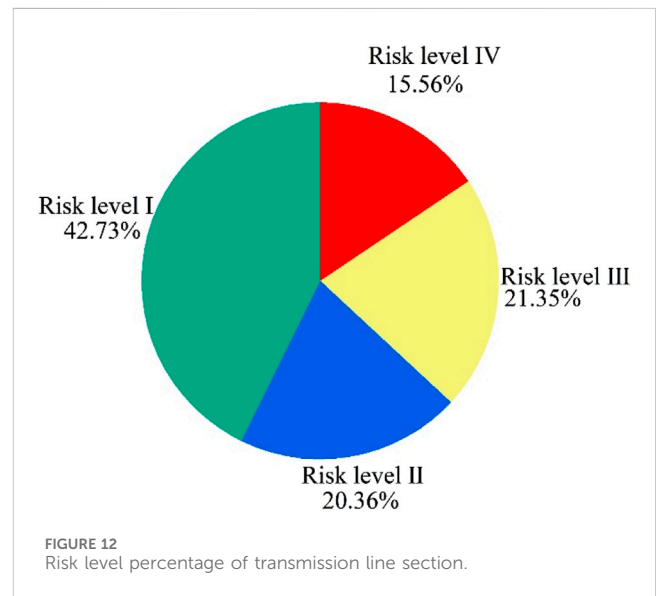


TABLE 3 The grading standard of risk levels.

Risk level	Level I	Level II	Level III	Level IV
R_i	[0,0.40]	(0.40,0.60]	(0.60,0.80]	(0.80,∞)
Representative color	Green	Blue	Yellow	red



large-scale or prolonged fires is diminished in these areas, resulting in lower probabilities of wildfire occurrences.

To verify the model’s applicability, the wildfire incidents spanning the years 2015–2020 were superimposed in the wildfire occurrence probability map. Specifically, 80.77% of the wildfires occurred in areas with a high probability of wildfire incidence (50%),

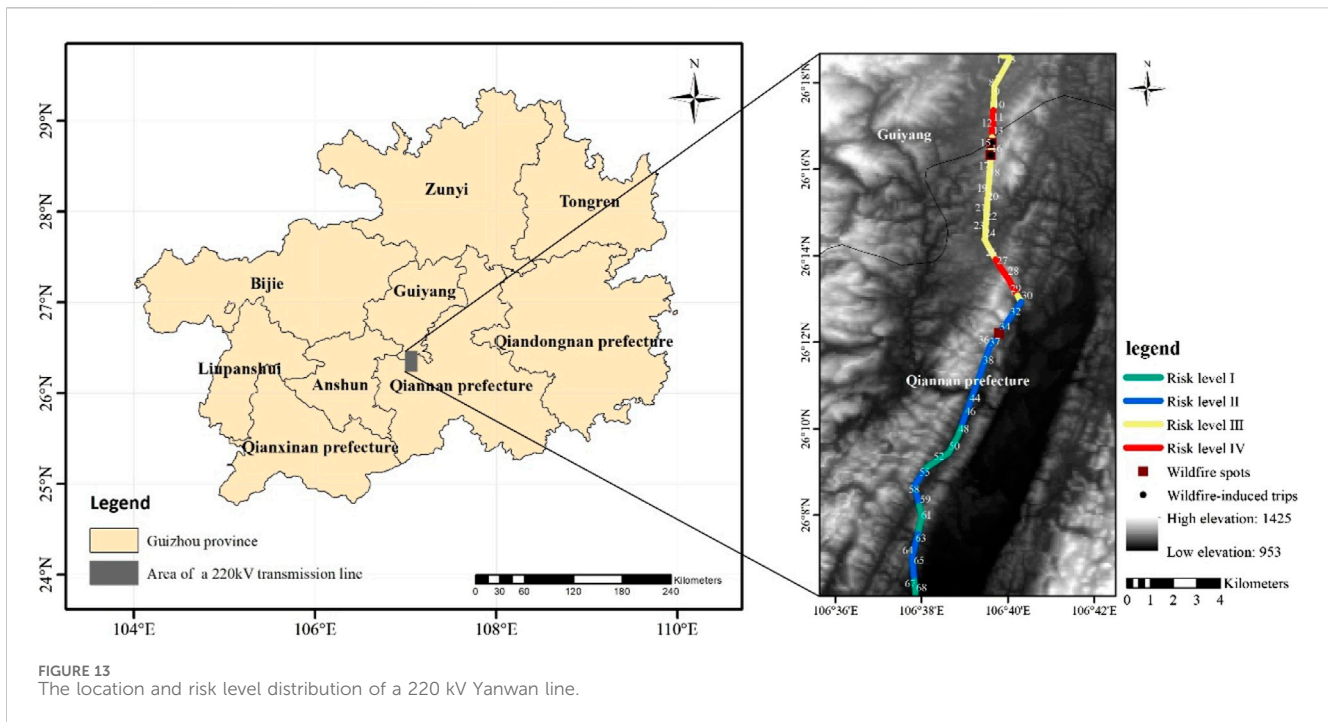


FIGURE 13 The location and risk level distribution of a 220 kV Yanwan line.

underscoring the high precision and predictive capability of the NBN model in forecasting wildfire events.

4.2 Wildfire-related tripping risk levels distribution of study area

Subsequently, based on the laser point cloud data, the insulation breakdown risks for all transmission line sections above 110 kV in the Guizhou Power Grid were computed. Multiplying these risks by the occurrence probability of wildfires yielded the final wildfire-related tripping risks for the transmission line sections. For visual representation, the risk values were categorized into four levels, each denoted by distinct colors as outlined in Table 3. The wildfire-related tripping risk levels in the Guizhou Power Grid were distributed as follows: 42.73%, 20.36%, 21.35%, and 15.56% respectively (see Figure 12). This signifies that the proposed method adeptly discriminates the wildfire risk distribution along transmission corridors.

4.3 Wildfire-related tripping risk analysis of 220 kV Yanwan line

To further illustrate the method’s efficacy, the 220 kV Yanwan line is taken as an illustrative case study. This transmission line spans from north to south, traversing the provincial capital city and its adjacent counties, comprising a total of 68 transmission towers. The distribution of risk levels among line sections is as follows: 17.91% for Level I, 38.81% for Level II, 34.33% for Level III, and 8.95% for Level IV (Figure 13). Specifically, line sections associated with the 10th-13th towers and the 26th-29th towers are identified as having a risk level IV. For line sections categorized as risk levels III and IV, it is imperative for the power supply bureau to enhance patrols and

monitoring in the vicinity, mitigating the potential impact of wildfires and averting tripping failures.

In the spring of 2020, two wildfire incidences transpired within the transmission corridor of the Yanwan line. One of them is monitored around 9:00 a.m. on February 28th within the line section encompassing the 34th-35th towers. Prompt intervention by the relevant departments led to its extinguishment by approximately 11:00 a.m. An assessment based on the probability distribution map of wildfire occurrences revealed a remarkably high probability of 97.89% for this specific line section. But the transmission line continued normal operation during the wildfire due to the underlying surface predominantly covered by grass, possessing a low fuel load of 1.25 t/hm². When ignited, the grass generated a maximum flame height of merely 0.43 m, causing minimal impact on the insulation of the transmission line. Consequently, the risk evaluation attributed a wildfire-induced tripping risk of 0.43, categorizing it as a level II risk within this line section.

Subsequently, at 14:00 p.m. on April 15th, another wildfire emerged within the transmission corridor, this time between the 14th and the 15th tower. Within a span of 2 h, the wildfire swiftly spread to the 16th tower, leading to a tripping failure of transmission line. The intensity of the blaze hindered successful reclosing, resulting in a partial power outage that inflicted substantial economic losses upon the Guizhou power grid. Investigation revealed the proliferation of oil-bearing coniferous forests beneath the transmission lines in these sections, with a canopy height of 15 m, leaving a minimal gap distance of 8 m from the transmission line. The wildfire-induced tripping risk was assessed at 0.65, thereby classifying it as a risk level III.

The actual consequences of the above two wildfire accidents coincided with wildfire-induced tripping risk of the corresponding line sections, indicating a good applicability of the proposed method. Currently, the model has successfully developed software and integrated into the Southern Power Grid Wildfire

Monitoring and Early Warning Center. This software performs automatic annual updates to the distribution map, detailing the occurrence probability of wildfires in each province and the associated tripping risk for transmission lines. It serves as a guide for local power grid operation and maintenance departments, directing heightened inspection efforts in areas prone to wildfires and specific line sections with elevated tripping risk. For the fire-spots monitored by satellites in real-time, this software provides the hazard level of the fire-spot on the transmission line. This information aids grid operation and maintenance departments in making informed decisions, including options for firefighting measures or the preemptive shutdown of transmission lines.

5 Conclusion

This paper introduces an innovative method for evaluating the risk of wildfire-induced tripping on transmission lines. The methodology comprises two key components: wildfire occurrence probability and insulation breakdown risk. In the first segment, a NBN model, coupled with extensive remote sensing data, is employed to rapidly estimate the likelihood of wildfire occurrence across each grid. By utilizing eight optimized wildfire-related factors, the model achieves a prediction accuracy of 80.77%. The ArcGIS software facilitates the visualization of wildfire probabilities, aiding relevant departments in swiftly identifying high-incidence areas. The second part focuses on assessing the insulation tripping risk of transmission lines. Leveraging Wang Zhengfei's combustion model, the flame height in the transmission corridor during a wildfire event is determined. The insulation of the transmission line is classified into two scenarios—Flame bridges entirety of air gap and Flame bridges part of air gap—based on the flame height. Through the refinement of the air breakdown model with flame parameters, the insulation breakdown risk of transmission lines is promptly assessed. This method provides a physical basis for wildfire-induced tripping risk assessment of transmission lines. Application in the Guizhou power grid demonstrates the model's robust applicability, offering valuable support for decision-making in grid about wildfire prevention and control.

References

- Benali, A., Ervilha, A. R., Sá, A. C. L., Fernandes, P. M., Pinto, R. M., Trigo, R. M., et al. (2016). Deciphering the impact of uncertainty on the accuracy of large wildfire spread simulations. *Sci. Total Environ.* 569, 73–85. doi:10.1016/j.scitotenv.2016.06.112
- Bian, H., Zhang, J., Li, R., Zhao, H., Wang, X., and Bai, Y. (2021). Risk analysis of tripping accidents of power grid caused by typical natural hazards based on FTA-BN model. *Nat. Hazards* 106, 1771–1795. doi:10.1007/s11069-021-04510-5
- Byram, G. M. (1959). *Combustion of forest fuels*. New York, USA: McGraw Hill.
- Castagna, J., Senatore, A., Bencardino, M., D'Amore, F., Sprovieri, F., Pirrone, N., et al. (2021). Multiscale assessment of the impact on air quality of an intense wildfire season in southern Italy. *Sci. Total Environ.* 761, 143271. doi:10.1016/j.scitotenv.2020.143271
- Chen, W., Zhou, Y., Zhou, E., Xiang, Z., and Lu, J. (2021). Wildfire risk assessment of transmission-line corridors based on Naïve Bayes network and remote sensing data. *Sensors* 21 (2), 634. doi:10.3390/s21020634
- Dian, S., Cheng, P., Ye, Q., Wu, J., Luo, R., Wang, C., et al. (2016). Integrating wildfires propagation prediction into early warning of electrical transmission line outages. *IEEE Access* 7, 27586–27603. doi:10.1109/access.2019.2894141
- Dios, V., Hedo, J., Camprubí, À. C., Thapa, P., Martínez del Castillo, E., Martínez de Aragón, J., et al. (2021). Climate change induced declines in fuel moisture may turn currently fire-free Pyrenean mountain forests into fire-prone ecosystems. *Sci. Total Environ.* 797, 149104. doi:10.1016/j.scitotenv.2021.149104
- Fonseca, J. R., Tan, A. L., Silva, R. P., Monassi, V., Assuncao, L., Junqueira, W., et al. (1990). Effects of agricultural fires on the performance of overhead transmission lines. *IEEE Trans. Power Deliv.* 5, 687–694. doi:10.1109/61.53071
- Gallimberti, I. (1979). The mechanism of the long spark formation. *J. De. Phys.* 7 (C7), C7-C193–C7-250. doi:10.1051/jphyscol:19797440
- Heskestad, G. (1998). Dynamics of the fire plume. *Math. Phys. Eng. Sci.* 356 (1748), 2815–2833. doi:10.1098/rsta.1998.0299
- Hoffmann, W., Schroeder, W., and Robert, B. J. (2003). Regional feedbacks among fire, climate, and tropical deforestation. *J. Geophys. Res.-search: Atmospheres* 108 (D23). doi:10.1029/2003JD003494
- Li, P., Huang, D., Ruan, J., Wei, H., Qin, Z., Long, M., et al. (2016). Influence of forest fire particles on the breakdown characteristics of air gap. *IEEE Trans. Dielectr. Electr. Insulation* 23, 1974–1984. doi:10.1109/tdei.2016.7556469

Data availability statement

The original contributions presented in the study are included in the article/Supplementary materials, further inquiries can be directed to the corresponding author.

Author contributions

EZ: Data curation, Investigation, Methodology, Resources, Software, Writing—original draft. LW: Investigation, Methodology, Validation, Writing—original draft. RW: Methodology, Software, Writing—review and editing. SL: Conceptualization, Methodology, Visualization, Writing—original draft. YZ: Data curation, Funding acquisition, Validation, Writing—original draft.

Funding

The author(s) declare financial support was received for the research, authorship, and/or publication of this article. We thank China Southern Power Grid Corporation Science and technology projects GDKJXM20222559. The authors also thank the National Natural Science Foundation of China for supporting this research under Contract Nos 52177015 and 51607012.

Conflict of interest

Authors EZ, LW, RW, SL, and YZ were employed by Electric Power Research Institute of Guangdong Power Grid Co., Ltd.

Publisher's note

All claims expressed in this article are solely those of the authors and do not necessarily represent those of their affiliated organizations, or those of the publisher, the editors and the reviewers. Any product that may be evaluated in this article, or claim that may be made by its manufacturer, is not guaranteed or endorsed by the publisher.

- Liu, Y., Li, B., Wu, C., Chen, B., and Zhou, T. (2021). Risk warning technology for the whole process of overhead transmission line trip caused by wildfire. *Nat. Hazards* 107 (1), 195–212. doi:10.1007/s11069-021-04579-y
- Lu, J., Guo, J., Yang, L., Feng, T., and Zhang, J. (2016a). Research and application of fire forecasting model for electric transmission lines incorporating meteorological data and human activities. *Math. Problems Eng.* 2016, 1–10. doi:10.1155/2016/9828676
- Lu, J., Zhou, T., Wu, C., Li, B., Tan, Y., and Zhu, Y. (2016b). Fault statistics and analysis of 220 kV and above power transmission line in province-level power grid. *High. Volt. Eng.* 42 (01), 200–207. doi:10.13336/j.1003-6520.hve.2016.01.026
- Millington, J., Romero-Calcerrada, R., Wainwright, J., and Perry, G. (2008). An agent-based model of mediterranean agricultural land-use/cover change for examining wildfire risk. *J. Artif. Soc. Soc. Simul.* 11 (4). doi:10.1016/j.insmathco.2008.05.013
- Mphale, K. M., Heron, M., Kethwaafetse, R., Letsholathebe, D., and Casey, R. (2010). Interferometric measurement of ionization in a grassfire. *Meteorology Atmos. Phys.* 106 (3), 191–203. doi:10.1007/s00703-010-0061-4
- Naido, P., and Swift, D. A. (1993). “Large particle initiated breakdown of an atmospheric air gap: relating to AC power line faults caused by sugar cane fires,” in *8th international symposium on high voltage engineering* (Yokohama, Japan: Japanese Electrotechnical Committee), 81–84.
- National Energy Administration of China (2016). *D/LT 1620—2016 Technical guide for wild fire risk forecast for overhead transmission lines*. Beijing, China: China Electric Power Press.
- Niu, R., Zhai, P. M., and Sun, M. (2006). Review of forest fire danger meteorological index and its construction method. *Mete-orological Mon.* 32 (12), 3–9. doi:10.3969/j.issn.1000-0526.2006.12.001
- Noble, I. R., Gill, A. M., and Bary, G. A. V. (1980). McArthur’s fire-danger meters expressed as equations. *Austral Ecol.* 5 (2), 201–203. doi:10.1111/j.1442-9993.1980.tb01243.x
- Perry, G. L. W. (1998). Current approaches to modelling the spread of wildland fire: a review. *Prog. Phys. Geogr. Environ.* 22 (2), 222–245. doi:10.1177/030913339802200204
- Pyne, S. J. (1984). *Introduction to wildland fire. Fire management in the United States*. Hoboken, USA: John Wiley and Sons.
- Requejo, C. D., Giné, G. R., and Pérez, F. A. (2019). Bayesian network modelling of hierarchical composite indicators. *Sci. Total Environ.* 668, 936–946. doi:10.1016/j.scitotenv.2019.02.282
- Rizk, F. A. M. (1989a). A model for switching impulse leader inception and breakdown of long air-gaps. *IEEE Trans. Power Deliv.* 4, 596–606. doi:10.1109/61.19251
- Rizk, F. A. M. (1989b). Switching impulse strength of air insulation: leader inception criterion. *IEEE Trans. Power Deliv.* 4, 2187–2195. doi:10.1109/61.35646
- Sherstyukov, B. (2002). “Index of forest fire,” in *Yearbook of weather, climate and ecology of moscow* (Moscow: Moscow State Univ Publ).
- Shi, S., Yao, C., Wang, S., and Han, W. (2018). A model design for risk assessment of line tripping caused by wildfires. *Sensors* 18 (6), 1941. doi:10.3390/s18061941
- State Grid Corporation of China (2016). *Q/GDW 11643—2016 Drawing guidelines for region distribution map of wildfires near overhead transmission lines*. Beijing, China: China Electric Power Press.
- Sun, T., Zhang, L., Chen, W., Tang, X., and Qin, Q. (2012). Mountains forest fire spread simulator based on geo-cellular automaton combined with Wang zhengfei velocity model. *IEEE J. Sel. Top. Appl. Earth Observations Remote Sens.* 6 (4), 1971–1987. doi:10.1109/jstars.2012.2231956
- Van, W., and Forest, P. (1987). “Development and structure of the Canadian forest fireweather index system,” in *Canadian forestry service forestry technical report* (Canada: Canadian Forestry Service).
- Wang, J., Yang, Y., Cui, D., Lei, M., Zhang, X., Wang, Q., et al. (2011). *GB/T 16927.1-2011, High-voltage test techniques - Part 1: general definitions and test requirements*. Beijing, China: China Standard Press.
- West, H. J. (1979). “Fire induced flashover of EHV transmission lines,” in *IEEE power apparatus and systems winter meeting* (New York: IEEE), 1142.
- William, A. H., Wilfrid, S., and Robert, B. J. (2003). Regional feedbacks among fire, climate, and tropical deforestation. *J. Geophys. Res.* 108 (D23). doi:10.1029/2003jd003494
- Woznicki, S. A., Baynes, J., Panlasigui, S., Mehaffey, M., and Neale, A. (2019). Development of a spatially complete floodplain map of the conterminous United States using random forest. *Sci. Total Environ.* 647, 942–953. doi:10.1016/j.scitotenv.2018.07.353
- Wu, Y., Xue, Y., Lu, J., Xie, Y., Xu, D., Li, W., et al. (2016). Space-time impact of forest fire on power grid fault probability. *Automation Electr. Power Syst.* 40 (03), 14–20. doi:10.7500/AEPS20151110015
- You, F., Chen, H., Zhang, L., Zhang, Y., Zhou, J., and Zhu, J. (2011). Experimental study on flashover of high-voltage transmission lines induced by wood crib fire. *Proc. CSEE* 31 (34), 192–197. doi:10.13334/j.0258-8013.pcsee.2011.34.021
- Zhou, H., Sun, L., Yang, Y., Liu, C., Liu, T., Xie, P., et al. (2018). Reduction of electric field strength by two species of trees under power transmission lines. *J. For. Res.* 29, 1415–1422. doi:10.1007/s11676-017-0541-1
- Zhou, T., Wu, C., Chen, H., Xi, C., Li, B., and Tan, Y. (2019). Temporal and spatial distribution laws of transmission line trips caused by wildfire for Hunan power grid. *Fire Sci. Technol.* 38 (3), 417–420. doi:10.3969/j.issn.1009-0029.2019.03.033